Most probable charge of fission products in 24 MeV proton induced fission of ^{238}U

H. Kudo, M. Maruyama, and M. Tanikawa*
Department of Chemistry, Faculty of Science, Niigata University, Niigata, Japan

T. Shinozuka and M. Fujioka
Cyclotron and Radioisotope Center, Tohoku University, Sendai, Japan
(Received 10 May 1996; revised manuscript received 25 April 1997)

The charge distributions of fission products in 24 MeV proton-induced fission of ^{238}U were measured by the use of an ion-guide isotope separator on line. The most probable charge (Z_p) of the charge distribution was discussed in view of the charge polarization in the fission process. It was found that Z_p mainly lies on the proton-rich side in the light mass region and on the proton-deficient side in the heavy mass region compared with the postulate of the unchanged charge distribution. The charge polarization was examined with respect to production Q values. [S0556-2813(98)04101-6]

PACS number(s): 25.85.Ge, 24.75.+i

I. INTRODUCTION

The process of nuclear charge division of a fissioning nucleus between two fragments is of great interest in connection with the mass splitting in nuclear fission. Wahl *et al.* proposed that the charge distribution of fission products is well represented by a normal Gaussian function [1]. Earlier experiments in thermal neutron-induced and spontaneous fission show that the width of the charge dispersion is not dependent essentially upon either the fissioning nucleus or the excitation energy [1–3]. Small deviations from the Gaussian curve have been explained due to the odd-even effects which enhance the yield of nuclei with even numbers of protons and/or neutrons [4,5]. Attempts have also been made to relate these yield deviations to the shell effects by which nuclei with magic numbers are favorably produced [1,5].

Several hypotheses about the most probable charge have been proposed. According to the unchanged charge distribution (UCD), primary fission fragments have the same proton-to-mass ratio as in the fissioning nucleus. If the charge in the fissioning nucleus is distributed homogeneously and the redistribution of the charge does not occur in the course of the fission process, the charge density of fission fragments will be the same as that of the fissioning nucleus. In this sense, the UCD hypothesis is straightforward and permits a simple method to estimate the most probable charge [6–8]. The equal charge displacement (ECD) states that the most probable charges for one fission fragment and for its complementary fragment lie an equal number of charge units away from the β stability line. This ECD hypothesis was empirically suggested by Glendenin [9] and seems to reproduce the most probable charge in low excitation fission [1,2,10]. In the minimum potential energy model (MPE), a nucleonic redistribution occurs such that a minimum in the sum of the nuclear potential energy and Coulomb repulsion energy is attained and fission proceeds along the minimum potential energy surface. This MPE hypothesis was proposed by Present [11] and found to describe the fission of ^{197}Au with 112 MeV ^{12}C rather well [12]. However, none of the various postulates have succeeded in becoming a general rule.

Many experimental studies have been carried out to determine the charge distribution in various reaction systems [1–4,13–20]. Most of them were performed using radiochemical separations [1–4,13–19] or by using an ordinary isotope separator [20]. The majority of fission products formed in low-energy fission of actinides are neutron-rich nuclides that have relatively short half-lives. Since the radiochemical analysis methods usually take a long time, it is difficult to measure the products with very short half-lives. Also the method using an ordinary isotope separator is not applicable to highly refractory elements. Mass-gated x-ray measurement also gives information about the charge distribution [21]. However, this method contains fairly large ambiguity in determining yields due to the nuclear de-excitation process resulting in large variations of x-ray fluorescence yields from isotope to isotope. In this sense, the direct measurement of nuclides of interest is superior to the x-ray measurement. And yet, up to now, the obtained nuclides were restricted to several masses and mostly situated on the neutron-deficient side of the charge distribution at each mass chain.

In the present work, the charge distributions in the proton-induced fission of ^{238}U were obtained by the use of an ion-guide isotope separator on-line (IGISOL). As IGISOL does not have an ordinary ion source and thus most difficulties arising from the ion source are not encountered. Using this method, very short-lived nuclides were measured with a reasonably high efficiency [22].

II. EXPERIMENT

A. Irradiation and mass separation

The experiments were performed by the use of the AVF cyclotron and IGISOL at the Cyclotron and Radioisotope Center in Tohoku University. The Tohoku IGISOL is composed of an ion-guide chamber, a mass separator, and a tape transport system [23]. The ion-guide chamber consists of an

*Present address: Faculty of Science, the University of Tokyo, Tokyo, Japan.

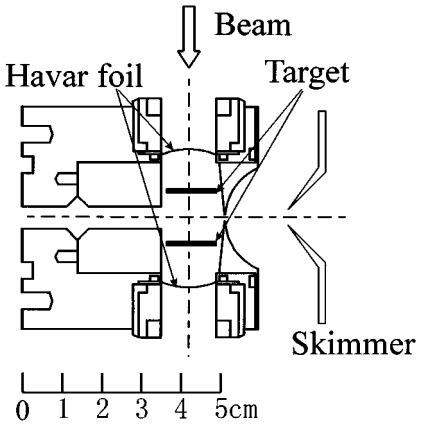

FIG. 1. Cross-sectional view of the IGISOL target chamber.

ion-guide vacuum chamber and an ion-guide target chamber. The chamber is separated from the cyclotron beam line by two titanium foil windows of 6.8 mg/cm^2 thickness at the entrance and the exit of the beam line, and evacuated by the large-capacity mechanical booster pumping system. The target chamber is separated by windows of 5 μm thick Havar foils from the vacuum area of the vacuum chamber and filled with helium buffer gas of about 140 mbar pressure. The cross-sectional view of the target chamber is shown in Fig. 1. The target in the target chamber consisted of two self-support foils of ^{238}U whose thicknesses were 20 mg/cm^2. Proton bombarding energy was 24 MeV at the point between the two target foils. The beam energy losses in the window foils and the target foils were calculated from the range-energy relationship [24]. The beam intensity was monitored by a Faraday cup equipped with a current integrator, and was checked at both the entrance and exit points of the target chamber in order to correct for the effect of the scattering in the window foils and the targets. The beam current was typically about 1.5 μA on target. In the present work, however, it was not necessary to measure a precise beam current, because only the relative cross sections of isobaric members were of interest.

Most of the helium gas from the target chamber is removed by differential pumping with a skimmer system. The electric field of around -500 V between the exit hole and the skimmer guides thermarized recoil ions in the extraction part of the mass separator. The ions are accelerated with the extraction field applied to the skimmer and the extraction electrode, and are introduced to the analyzing magnet after being made into a parallel beam by two lens systems. Mass separated ions are collected on an aluminized Mylar tape of the tape transport system which is controlled by a microcomputer. For the adjustment of the mass separator O^+ ions were used and the optimum magnetic field was determined by measuring the γ-ray activities of fission products at each mass number.

B. Measurement

The identification and the determination of the radioactivities of fission products were made by a γ-ray spectrometry using two high-purity Ge detectors coupled to 4 K-channel pulse height analyzers. One detector was positioned just behind the collecting point of transported fission products, and used for the measurement of accumulating radioactivities. The other was set about 40 cm away from the first detector along the collection tape, and used for a growth and decay measurement [25]. It took 0.3 s to move the collection tape between the two measuring positions. The energy resolutions full width at half maximum of the two detectors were 2.1 and 2.8 keV for the 1332 keV γ ray of ^{60}Co, respectively. The calibrations of γ-ray energy and detection efficiency for the energy range from 50 to about 3000 keV were performed using a set of γ reference sources (^{22}Na, ^{54}Mn, ^{57}Co, ^{60}Co, ^{137}Cs, ^{133}Ba, and ^{241}Am) and handmade sources of ^{56}Co and ^{152}Eu. In order to avoid loss from the photopeak through summing of detector pulses, the detectors were positioned at more than 2 cm from the source position.

For the growth and decay measurement the time interval of the tape transportation was varied from 5 s to 30 min according to the half-lives of nuclides of interest. In order to get a reasonable γ-ray photopeak area of the nuclide of interest, counting cycles were repeated from 10 to 5000 times which correspond to about 2–9 h measurements. For the decay analysis, γ-ray spectral data were recorded on a magnetic tape event by event together with the time information of a Multi Channel Scaler (MCS), and monitored by the GPIB-based fast data acquisition system [26]. The time signal of the end of the tape movement was used for the trigger pulse of MCS.

For some nuclides, γ-ray measurements were performed by a simple accumulation method. In this method, only the first detector was used. The activity was simply measured for 2–3 h through the irradiation period, and the tape transport system was used only to discard the radioactivities of long-lived nuclides which disturb the spectra as a background activity.

C. Data treatment

Most of fission products are on the neutron-rich side of the β stability line. They will become stable after successive β decays. Therefore, in order to deduce the independent yield from the measured radioactivity, it is necessary to correct for the contribution from precursors. For the growth and decay analysis, the event-by-event data were converted to 3–10 consecutive singles spectra in time sequence according to the MCS data. The time interval corresponding to each spectrum depends on the half-life of the nuclide of interest. The obtained singles spectra were analyzed by the program SAMPO [27] and an originally developed program which works interactively.

The obtained radioactivities were converted to either partial cumulative yields or independent yields as follows. After the end of collection, the following differential equations hold for the members of a given decay chain:

$$\frac{dN_1}{dt} = -N_1\lambda_1, \tag{1}$$

$$\frac{dN_i}{dt} = N_{i-1}\lambda_{i-1} - N_i\lambda_i, \quad i = 2,3,..., \tag{2}$$

where $N_1, N_2, N_3, \ldots$ are the number of nuclei at time t, and

$\lambda_1,\lambda_2,\lambda_3,\ldots$ are the characteristic decay constants. These differential equations can be easily solved and activities are given by

$$A_1 = A_{10}\exp(-\lambda_1 t), \tag{3}$$

$$A_2 = A_{10}\frac{\lambda_2}{\lambda_2-\lambda_1}\{\exp(-\lambda_1 t)-\exp(-\lambda_2 t)\} + A_{20}\exp(-\lambda_2 t), \tag{4}$$

$$A_3 = A_{10}\lambda_2\lambda_3\left\{\frac{\exp(-\lambda_1 t)}{(\lambda_2-\lambda_1)(\lambda_3-\lambda_1)} + \frac{\exp(-\lambda_2 t)}{(\lambda_1-\lambda_2)(\lambda_3-\lambda_2)} + \frac{\exp(-\lambda_3 t)}{(\lambda_1-\lambda_3)(\lambda_2-\lambda_3)}\right\} + A_{20}\frac{\lambda_3}{\lambda_3-\lambda_2}\{\exp(-\lambda_2 t) - \exp(-\lambda_3 t)\} + A_{30}\exp(-\lambda_3 t)\ldots, \tag{5}$$

where $A_1,A_2,A_3,\ldots$ are the radioactivities at the time t and $A_{10},A_{20},A_{30},\ldots$ are the activities at the end of collection. The obtained activities at the end of collection were converted to corresponding cross sections by correcting for saturation conditions. The next differential equations hold during the period of collection:

$$\frac{dN_1}{dt} = N_0\sigma_1\varepsilon_1\phi - N_1\lambda_1, \tag{6}$$

$$\frac{dN_i}{dt} = N_0\sigma_i\varepsilon_i\phi + N_{i-1}\lambda_{i-1} - N_i\lambda_i \qquad i = 2,3,\ldots \tag{7}$$

where N_0 is the number of the target nuclei, $\sigma_1,\sigma_2,\sigma_3,\ldots$ are the cross sections, $\varepsilon_1,\varepsilon_2,\varepsilon_3,\ldots$ are the transport efficiencies in IGISOL, and ϕ is the proton beam flux. By solving these differential equations, the next equations are derived:

$$A_{10} = N_0\sigma_1\varepsilon_1\phi\{1-\exp(-\lambda_1 t)\}, \tag{8}$$

$$A_{20} = N_0\sigma_1\varepsilon_1\phi\left[\frac{\lambda_2}{\lambda_2-\lambda_1}\{1-\exp(-\lambda_1 t)\} + \frac{\lambda_1}{\lambda_1-\lambda_2}\{1-\exp(-\lambda_2 t)\}\right] + N_0\sigma_2\varepsilon_2\phi\{1-\exp(-\lambda_2 t)\}, \tag{9}$$

$$A_{30} = N_0\sigma_1\varepsilon_1\phi\left[\frac{\lambda_2\lambda_3}{(\lambda_2-\lambda_1)(\lambda_3-\lambda_1)}\{1-\exp(-\lambda_1 t)\} + \frac{\lambda_1\lambda_3}{(\lambda_1-\lambda_2)(\lambda_3-\lambda_2)}\{1-\exp(-\lambda_2 t)\} + \frac{\lambda_1\lambda_2}{(\lambda_1-\lambda_3)(\lambda_2-\lambda_3)} \times \{1-\exp(-\lambda_3 t)\}\right] + N_0\sigma_2\varepsilon_2\phi\left[\frac{\lambda_3}{\lambda_3-\lambda_2}\{1-\exp(-\lambda_2 t)\} + \frac{\lambda_2}{\lambda_2-\lambda_3}\{1-\exp(-\lambda_3 t)\}\right] + N_0\sigma_3\varepsilon_3\phi\{1-\exp(-\lambda_3 t)\}\ldots . \tag{10}$$

Thus, the relative independent yields, $N_0\sigma_i\varepsilon_i$ can be obtained by substituting A_{i0}'s in Eqs. (3)–(5) for Eqs. (8)–(10).

For the simple accumulation method, Eqs. (8)–(10) were integrated over the collection time T:

$$C_1 = N_0\sigma_1\varepsilon_1\phi\left[T - \frac{1}{\lambda_1}\{1-\exp(-\lambda_1 T)\}\right], \tag{11}$$

$$C_2 = N_0\sigma_1\varepsilon_1\phi\left[T - \frac{\lambda_2}{\lambda_1(\lambda_2-\lambda_1)}\{1-\exp(-\lambda_1 T)\} - \frac{\lambda_1}{\lambda_2(\lambda_1-\lambda_2)}\{1-\exp(-\lambda_2 T)\}\right] + N_0\sigma_2\varepsilon_2\phi\left[T - \frac{1}{\lambda_2}\{1-\exp(-\lambda_2 T)\}\right], \tag{12}$$

$$C_3 = N_0\sigma_1\varepsilon_1\phi\left[T - \frac{\lambda_2\lambda_3}{\lambda_1(\lambda_2-\lambda_1)(\lambda_3-\lambda_1)}\{1-\exp(-\lambda_1 T)\} - \frac{\lambda_1\lambda_3}{\lambda_2(\lambda_1-\lambda_2)(\lambda_3-\lambda_2)}\{1-\exp(-\lambda_2 T)\} - \frac{\lambda_1\lambda_2}{\lambda_3(\lambda_1-\lambda_3)(\lambda_2-\lambda_3)}\{1-\exp(-\lambda_3 T)\}\right] + N_0\sigma_2\varepsilon_2\phi\left[T - \frac{\lambda_3}{\lambda_2(\lambda_3-\lambda_2)}\{1-\exp(-\lambda_2 T)\} - \frac{\lambda_2}{\lambda_3(\lambda_2-\lambda_3)}\{1-\exp(-\lambda_3 T)\}\right] + N_0\sigma_3\varepsilon_3\phi\left[T - \frac{1}{\lambda_3}\{1-\exp(-\lambda_3 T)\}\right]\ldots, \tag{13}$$

where $C_1, C_2, C_3, \ldots$ are the number of disintegration during the collection.

If there is a branch of disintegration, the corresponding terms in the above equations are multiplied by the branching ratios. The nuclear data used for the analysis are listed in Table I with quoted references [28–64].

Since the time taken to transport the products from the target chamber to the collecting position is short enough in comparison with the half-lives of the nuclides of interest, the decay during the period between production and collection was neglected in the above calculation.

III. RESULTS AND DISCUSSION

A. Relative yield of fission product

The relative yields of 143 nuclides in 40 mass chains were measured in the system of 24 MeV proton-induced fission of ^{238}U by the use of IGISOL. The results are summarized in Table I, where the relative yields are expressed as fractional yields. For the conversion of the relative yield into the fractional yield, it is necessary to evaluate the chain yield for each mass number. The chain yields were estimated assuming a Gaussian charge distribution with the parameters described in the next section. The mass number of the observed nuclides ranges from 82 to 149, including symmetric fission products. The half-lives of these nuclides range from 0.320 s (^{120}Ag) to 13.16 days (^{136}Cs). In particular, it is noteworthy to have determined the yields of 76 nuclides having half-lives less than a minute. Such short-lived nuclides could not have been measured using conventional methods over such a wide range of mass numbers. The errors in the yields were estimated from counting statistics, uncertainties in half-lives and errors propagated from parent nuclides if any.

The obtained yields include the transport efficiency in IGISOL which may differ element by element and/or mass chain to mass chain. The difference of the transport efficiency in IGISOL can be eliminated in the following way.

To begin with, in IGISOL we can measure only the fraction of produced fission fragments that are thermalized in a helium buffer gas. The recoil ranges of fission fragments differ from one another due to the wide variety of mass numbers, atomic numbers, and kinetic energies of fission fragments. The position of the effective region in the target varies with the recoil range of a fragment. However, the differences of the effective target thicknesses are expected to be small for neighboring fragments of interest.

Next, the transport efficiency may be affected by both operating conditions of the mass separator and the chemical properties of the elements. The former defined as a physical transport efficiency ε_p comes from the operating conditions of the mass separator such as the width of the defining slit. The latter defined as a chemical transport efficiency ε_c is related to the thermal equilibrium of ions in a helium atmosphere. The transport efficiency also depends on the proton beam intensity [65]. Although the magnitudes of the transport efficiencies were considerably affected by the change of the beam intensity, the ratios of the yields between the members of the same mass chain were quite constant. Therefore, the dependence of the beam intensity could be included in ε_p. Since the overall transport efficiency ε_t can be regarded as the product of ε_p and ε_c, the observed yield of the nuclide of interest P is expressed as $\varepsilon_p \varepsilon_c N_0 \sigma$.

For the nuclides with the same mass number A_1, the transport efficiency ε_p arising from the operating conditions of the mass separator is considered to be the same, because the members of a given isobar chain are simultaneously measured in a single experimental run. Therefore, the ratio between the yields of isobars Z_1 and Z_2 includes only ε_c,

$$\frac{P_{A_1Z_1}}{P_{A_1Z_2}} = \frac{\varepsilon_{c_{Z_1}} \cdot \sigma_{A_1Z_1}}{\varepsilon_{c_{Z_2}} \cdot \sigma_{A_1Z_2}}. \tag{14}$$

In the same way, for the other mass number A_2, the next equation holds,

$$\frac{P_{A_2Z_1}}{P_{A_2Z_2}} = \frac{\varepsilon_{c_{Z_1}} \cdot \sigma_{A_2Z_1}}{\varepsilon_{c_{Z_2}} \cdot \sigma_{A_2Z_2}}. \tag{15}$$

Since the nuclides with the same atomic number have the same chemical property, the corresponding ε_c can be regarded as the same. Consequently, by taking the ratio of Eqs. (14) and (15), the transport efficiency in IGISOL can be eliminated

$$\frac{P_{A_1Z_1} \cdot P_{A_2Z_2}}{P_{A_2Z_1} \cdot P_{A_1Z_2}} = \frac{\sigma_{A_1Z_1} \cdot \sigma_{A_2Z_2}}{\sigma_{A_2Z_1} \cdot \sigma_{A_1Z_2}}. \tag{16}$$

Therefore, if two kinds of isotopes are measured in different mass chains, one can extract the relationship between the yields independent of the transport efficiency in IGISOL.

B. Evaluation of the most probable charge

Empirically, the charge dispersion of fission products has been well represented by a Gaussian distribution [1]. The theoretical calculation with the asymmetric two-center shell model also gives a Gaussian charge distribution [66,67]. In low-energy fission, such as thermal-neutron-induced and spontaneous fission, deviations from a Gaussian have been observed. This is ascribed to the odd-even nature of nuclides [5]. In charged-particle-induced fission, however, the odd-even effect is presumed not to appear because the high excitation energy of the fissioning nuclei should wash out the effect. A great reduction of the odd-even effect has been observed to occur when only an extra 3 MeV is added in the system of neutron-induced fission of ^{235}U [68]. The same kind of reduction of the odd-even effect is observed in photo-induced fission of ^{238}U [69]. In the present work, therefore, the analysis of the charge dispersion was performed by assuming the following Gaussian function:

$$\sigma_{AZ} = \frac{\sigma_A}{(C\pi)^{1/2}} \exp\left(- \frac{(Z - Z_p)^2}{C} \right), \tag{17}$$

where σ_{AZ} is the independent yield of the nuclide with an atomic charge Z and a mass number A, σ_A is the chain yield of the mass chain A, Z_p is the most probable charge, and C is the width parameter of the distribution.

If the width parameters of the charge distributions for different mass chains are constant as reported earlier [1–3],

TABLE I. Nuclear data used for the analysis and the obtained relative yields. Only a main characteristic γ ray of each nuclide is listed.

Nuclide	$T_{1/2}$	E_γ (keV)	I_γ (%)	Ref.	Yield[a]	Type[b]	Method[c]
^{82}Ge	4.6 s	1091.9	90.	[28]	0.053±0.003	*C*	GD
^{82b}As	13.6 s	343.5	57.6	[28]	0.088±0.003	*I*	GD
^{82a}As	19.1 s	654.4	15.1	[28]	0.329±0.031	*I*	GD
^{83}As	13.4 s	734.6	43.	[29]	0.451±0.016	*C*	GD
^{83m}Se	22.3 min	1030.6	20.6	[29]	0.054±0.030	*I*	GD
^{83g}Se	70.1 s	356.7	69.9	[29]	0.418±0.052	*I*	GD
^{84}As	5.5 s	1455.1	49.	[30]	0.071±0.002	*C*	GD
^{84}Se	3.1 min	408.2	100.	[30]	0.564±0.003	*I*	GD
^{84m}Br	6 min	424.0	100.	[30]	0.044±0.001	*I*	GD
^{84g}Br	31.8 min	1897.6	14.7	[30]	0.011±0.003	*I*	GD
^{87}Br	55.69 s	1419.8	32.	[31]	0.036±0.052	*C*	GD
^{87}Kr	76.31 min	402.6	49.6	[31]	0.357±0.110	*I*	GD
^{87m}Sr	2.81 h	388.4	81.8	[31]	0.175±0.084	*I*	GD
^{88}Se	1.52 s	159.2	10.6	[32]	0.215±0.012	*C*	GD
^{88}Br	16.5 s	775.3	63.	[32]	0.500±0.030	*I*	GD
^{88}Kr	2.84 h	196.3	26.	[32]	0.438±0.061	*I*	GD
^{88}Rb	17.78 min	1836.0	21.4	[32]	0.163±0.014	*I*	GD
^{90}Br	1.92 s	707.1	38.	[33]	0.064±0.004	*C*	GD
^{90}Kr	32.3 s	1118.7	36.2	[33]	0.178±0.006	*I*	GD
^{90m}Rb	4.3 min	824.2	8.64	[33]	0.459±0.006	*I*	GD
^{90g}Rb	2.6 min	831.7	27.8	[33]	0.102±0.035	*I*	GD
^{91}Kr	8.57 s	108.8	43.5	[34]	0.017±0.001	*C*	GD
^{91}Rb	58.4 s	93.6	33.7	[34]	0.524±0.016	*I*	GD
^{91}Sr	9.52 h	1024.3	33.4	[34]	0.263±0.047	*I*	GD
^{91m}Y	49.71 min	555.6	94.9	[34]	0.003±0.001	*I*	GD
^{92}Kr	1.85 s	142.4	66.	[35]	0.011±0.002	*C*	GD
^{92}Rb	4.5 s	814.7	8.	[35]	0.249±0.092	*I*	GD
^{92}Sr	2.71 h	1383.9	90.	[35]	0.559±0.155	*I*	GD
^{93}Kr	1.29 s	266.8	20.3	[36]	0.008±0.001	*C*	GD
^{93}Rb	5.7 s	986.2	4.43	[36]	0.500±0.050	*I*	GD
^{93}Sr	7.423 min	590.3	65.7	[36]	0.064±0.056	*I*	GD
^{94}Rb	2.702 s	836.9	87.1	[37]	0.359±0.010	*C*	GD
^{94}Sr	75.1 s	1427.6	94.2	[37]	0.518±0.044	*I*	GD
^{95}Sr	25.1 s	685.9	24.	[38]	0.481±0.102	*C*	GD
^{95}Y	10.3 min	954.2	19.	[38]	0.454±0.231	*I*	GD
^{97}Sr	0.42 s	1905.0	28.	[39]	0.293±0.011	*C*	SA
^{97m}Y	1.23 s	161.4	70.7	[39]	0.389±0.006	*I*	SA
^{97g}Y	3.5 s	3287.7	18.1	[39]	0.162±0.024	I	SA
^{99}Y	1.47 s	121.8	43.8	[40]	0.136±0.004	*C*	SA
^{99}Zr	2.1 s	469.1	55.2	[40]	0.187±0.013	*I*	SA
^{99m}Nb	2.6 min	253.3	3.71	[40]	0.348±0.026	*I*	SA
^{99g}Nb	15 s	137.7	90.6	[40]	0.227±0.019	*I*	SA
^{102}Mo	11.2 min	211.7	3.82	[33]	0.938±0.011	*C*	GD
^{102m}Tc	4.35 min	628.1	25.2	[33]	0.043±0.002	*I*	GD
^{102g}Tc	5.28 s	475.1	6.25	[33]	0.020±0.005	*I*	GD
^{108}Tc	5.17 s	242.2	82.4	[41]	0.469±0.001	*C*	GD
^{108}Ru	4.55 min	(434.1	43.)[d]	[41]	0.465±0.010	*I*	GD
^{108b}Rh	6 min	581.1	59.	[41]	0.019±0.001	*I*	GD
^{108a}Rh	16.8 s	434.1	43.	[41]	0.005±0.002	*I*	GD
^{116}Pd	12.72 s	114.7	88.	[33]	0.487±0.004	*C*	GD
^{116m}Ag	10.4 s	1028.9	30.	[33]	0.290±0.003	*I*	GD
^{116g}Ag	2.68 min	699.3	10.9	[33]	0.161±0.024	*I*	GD
^{116m}In	2.18 s	162.4	36.6	[33]	0.037±0.006	*I*	GD
^{116m}In	54.15 min	416.9	26.2	[33]	0.039±0.012	*I*	GD
^{119}Ag	2.1 s	626.4	10.7	[33]	0.438±0.013	*C*	GD

TABLE I. (*Continued.*)

Nuclide	$T_{1/2}$	E_γ (keV)	I_γ (%)	Ref.	Yield[a]	Type[b]	Method[c]
^{119m}Cd	2.2 min	1025.0	25.	[33]	0.420 ± 0.005	*I*	GD
^{119g}Cd	2.69 min	292.9	41.	[33]	0.061 ± 0.010	*I*	GD
^{120}Cd	50.8 s	(1172.5	20.)[d]	[33,42]	0.176 ± 0.004	*C*	GD
^{120c}In	47.3 s	89.9	77.6	[42]	0.284 ± 0.003	*I*	GD
^{120b}In	46.2 s	863.7	32.5	[42]	0.129 ± 0.011	*I*	GD
^{120a}In	3.08 s	1172.5	19.	[42]	0.145 ± 0.049	*I*	GD
^{121}Ag	0.72 s	341.6	30.9	[43]	0.040 ± 0.003	*C*	GD
^{121m}Cd	8.3 s	1020.9	18.9	[44]	0.260 ± 0.004	*I*	GD
^{121g}Cd	13.5 s	324.2	49.5	[44]	0.073 ± 0.003	*I*	GD
^{121g}In	23.1 s	925.6	87.	[33]	0.746 ± 0.054	*I*	GD
^{122}Cd	5.24 s	1140.3	39.	[33,45]	0.491 ± 0.016	*C*	GD
^{122a}In	10.8 s	407.3	7.8	[45]	0.283 ± 0.010	*I*	GD
^{122b}In	10.3 s	1190.3	20.	[45]	0.079 ± 0.010	*I*	GD
^{122a}In	1.5 s	1013.1	2.7	[45]	0.078 ± 0.026	*I*	GD
^{124}Cd	0.9 s	179.9	49.9	[46]	0.135 ± 0.010	*C*	GD
^{124b}In	2.4 s	1359.9	38.8	[46]	0.413 ± 0.002	*I*	GD
^{124a}In	3.17 s	997.8	21.1	[46]	0.126 ± 0.015	*I*	GD
^{126}Cd	0.51 s	260.1	89.6	[33,47]	0.042 ± 0.001	*C*	GD
^{126b}In	1.45 s	111.8	88.	[47]	0.204 ± 0.009	*I*	GD
^{126a}In	1.5 s	969.6	14.9	[47]	0.179 ± 0.013	*I*	GD
^{128b}In	0.9 s	1867.0	32.3	[48]	0.023 ± 0.006	*C*	GD
^{128a}In	0.9 s	1168.8	50.3	[48]	0.016 ± 0.014	*C*	GD
^{128m}Sn	6.5 s	831.5	100.	[48]	0.193 ± 0.003	*I*	GD
^{128g}Sn	59.1 min	482.3	58.	[48]	0.177 ± 0.011	*I*	GD
^{128m}Sb	10.4 min	314	91.6	[48]	0.082 ± 0.005	*I*	GD
^{128g}Sb	9.01 h	526.5	45.	[48]	0.415 ± 0.066	*I*	GD
^{130m}Sn	1.7 min	144.9	34.	[33]	0.022 ± 0.001	*C*	GD
^{130g}Sn	3.72 min	192.5	71.	[33]	0.043 ± 0.001	*I*	GD
^{130b}Sb	6.3 min	1017.5	30.	[33]	0.167 ± 0.005	*I*	GD
^{130a}Sb	40 min	330.9	78.	[33]	0.264 ± 0.004	*I*	GD
^{130m}I	9 min	536.1	16.7	[33]	0.038 ± 0.007	*I*	GD
^{130g}I	12.36 h	668.5	96.1	[33]	0.179 ± 0.024	*I*	GD
^{131}Sb	23 min	943.4	44.	[49]	0.547 ± 0.024	*C*	GD
^{131g}Te	25 min	149.7	68.9	[49]	0.130 ± 0.030	*I*	GD
^{132}Sn	40 s	340.8	43.2	[33]	0.0041 ± 0.0004	*C*	SA
^{132b}Sb	2.8 min	989.6	15.	[33]	0.038 ± 0.002	*I*	SA
^{132a}Sb	4.2 min	1041.5	18.	[33]	0.026 ± 0.002	*I*	SA
^{132}Te	78.2 h	228.2	88.1	[33]	0.482 ± 0.053	*I*	SA
^{132m}I	83.6 min	599.8	13.2	[33]	0.305 ± 0.014	*I*	SA
^{132g}I	2.3 h	522.7	16.1	[33]	0.088 ± 0.012	*I*	SA
^{134}Te	41.8 min	210.5	22.5	[50]	0.266 ± 0.002	*C*	GD
^{134m}I	3.69 min	271.9	79.	[50]	0.333 ± 0.006	*I*	GD
^{134g}I	52.6 min	1072.5	15.	[50]	0.225 ± 0.007	*I*	GD
^{135}Te	19 s	603.5	37.	[51]	0.021 ± 0.001	*C*	GD
^{135}I	6.57 h	1260.4	28.9	[51]	0.790 ± 0.041	*I*	GD
^{135m}Xe	15.29 min	526.6	80.5	[51]	0.151 ± 0.001	*I*	GD
^{135g}Xe	9.14 h	249.8	90.2	[51]	0.059 ± 0.002	*I*	GD
^{136}Te	17.5 s	334.0	18.8	[52]	0.054 ± 0.009	*C*	GD
^{136b}I	46.9 s	381.4	99.8	[52]	0.176 ± 0.003	*I*	GD
^{136a}I	83.4 s	1321.1	24.8	[52]	0.039 ± 0.012	*I*	GD
^{136}Cs	13.16 days	818.5	99.7	[52]	0.202 ± 0.003	*I*	GD
^{138}I	6.41 s	588.8	60.	[53]	0.041 ± 0.006	*C*	SA
^{138}Xe	14.08 min	258.4	31.5	[53]	0.211 ± 0.022	*I*	SA
^{138m}Cs	2.9 min	191.7	15.4	[53]	0.479 ± 0.045	*I*	SA
^{138g}Cs	32.2 min	1009.8	29.8	[53]	0.085 ± 0.038	*I*	SA

TABLE I. (*Continued.*)

Nuclide	$T_{1/2}$	E_γ (keV)	I_γ (%)	Ref.	Yield[a]	Type[b]	Method[c]
^{139}Xe	39.68 s	218.6	52.	[54]	0.087 ± 0.008	*C*	GD
^{139}Cs	9.27 min	1283.2	7.7	[54]	0.566 ± 0.050	*I*	GD
^{139}Ba	1.38 h	165.8	23.8	[54]	0.266 ± 0.032	*I*	GD
^{140}Xe	13.6 s	805.5	20.	[55]	0.009 ± 0.003	*C*	GD
^{140}Cs	63.7 s	908.4	7.89	[55]	0.192 ± 0.021	*I*	GD
^{141}Xe	1.73 s	909.4	13.3	[56]	0.062 ± 0.005	*C*	GD
^{141}Cs	24.94 s	561.6	4.7	[56]	0.545 ± 0.021	*I*	GD
^{141}Ba	18.27 min	190.3	47	[56]	0.281 ± 0.031	*I*	GD
^{142}Ba	10.6 min	255.3	21.1	[57]	0.616 ± 0.025	*C*	GD
^{142}La	91.1 min	641.3	47.4	[57]	0.353 ± 0.078	*I*	GD
^{143}Cs	1.78 s	195.5	12.6	[58]	0.206 ± 0.020	*C*	GD
^{143}Ba	14.5 s	211.5	24.9	[58]	0.543 ± 0.029	*I*	GD
^{143}La	14.2 min	643.7	1.55	[58]	0.517 ± 0.207	*I*	GD
^{143}Ce	33 h	293.3	42.8	[58]	0.055 ± 0.055	*I*	GD
^{144}Ba	11.5 s	388.2	13.5	[59]	0.479 ± 0.077	*C*	GD
^{144}La	40.8 s	397.4	94.3	[59]	0.455 ± 0.044	*I*	GD
^{145}Cs	0.594 s	175.4	15.6	[60]	0.030 ± 0.002	*C*	GD
^{145}Ba	4.31 s	96.6	7.73	[60]	0.233 ± 0.012	*I*	GD
^{145}La	24.8 s	355.8	3.83	[60]	0.543 ± 0.047	*I*	GD
^{145}Ce	3.01 min	724.2	58.9	[60]	0.223 ± 0.017	*I*	GD
^{146}Ba	2.2 s	251.2	18	[61,62]	0.030 ± 0.012	*C*	GD
^{146m}La	10 s	409.9	87	[61]	0.225 ± 0.004	*I*	GD
^{146g}La	6.27 s	258.5	76	[61]	0.106 ± 0.006	*I*	GD
^{146}Ce	13.52 min	316.7	51	[61,62]	0.349 ± 0.009	*I*	GD
^{146}Pr	24.15 min	453.9	48	[62]	0.346 ± 0.015	*I*	GD
^{147}La	4.48 s	117.6	15	[33]	0.289 ± 0.029	*C*	GD
^{147}Ce	56.4 s	268.7	5.5	[33]	0.555 ± 0.061	*I*	GD
^{148}La	1.05 s	158.5	56	[63]	0.096 ± 0.015	*C*	GD
^{148}Ce	56 s	269.5	17	[63]	0.761 ± 0.023	*I*	GD
^{148b}Pr	2 min	450.8	50	[63]	0.050 ± 0.022	*I*	GD
^{148a}Pr	2.27 min	301.7	61	[63]	0.201 ± 0.005	*I*	GD
^{149}Pr	2.26 min	138.5	1.02	[64]	0.884 ± 0.041	*C*	GD
^{149}Nd	1.72 h	211.3	25.9	[64]	0.115 ± 0.084	*I*	GD

[a]Expressed as fractional yields in each mass chain.
[b]*C* indicates cumulative yield, *I* indicates independent yield.
[c]GD indicates growth and decay analysis, SA indicates the simple accumulation method.
[d]Obtained from daughter activity.

the difference dZ_p of the most probable charges between mass numbers A_1 and A_2 can be expressed as

$$dZ_p \equiv Z_{p_{A_1}} - Z_{p_{A_2}} = \frac{C}{2(Z_1 - Z_2)} \cdot \ln\left(\frac{\sigma_{A_1 Z_1} \cdot \sigma_{A_2 Z_2}}{\sigma_{A_1 Z_2} \cdot \sigma_{A_2 Z_1}}\right)$$
$$= \frac{C}{2(Z_1 - Z_2)} \cdot \ln\left(\frac{P_{A_1 Z_1} \cdot P_{A_2 Z_2}}{P_{A_1 Z_2} \cdot P_{A_2 Z_1}}\right). \quad (18)$$

As a result, the difference dZ_p is given in a unit of the width parameter C. When more than two nuclides are measured for A_1 and A_2, several combinations of Z_1 and Z_2 are possible in the evaluation of dZ_p. In those cases, a least-squares method was applied. The same kind of the data treatment is applicable in the analysis of the width parameter in order to eliminate the IGISOL transport efficiency. If three identical elements are observed at different mass chains, the difference of the reciprocals of width parameters, $1/C_{A_1} - 1/C_{A_2}$, can be evaluated in principle. However, due to the large errors, we could not obtain a significant result in the present work.

The resulting information about the most probable charges is based only on their differences dZ_p, but the transport efficiency in IGISOL is eliminated as described above. The obtained dZ_p's are not constant and some of them are negative with increasing mass number. For $A = 128$ to 149, a series of dZ_p was obtained as a function of mass number. Therefore, if at least two of the most probable charges are known in this mass region, other Z_p's can be evaluated. A set of the obtained dZ_p for the heavy fragments was transformed to the most probable charges by a least-squares method with the known most probable charges of $A = 132$, 134, 136, and 148 which were interpolated form the reported data by Umezawa, Baba, and Baba [17]. In this calculation the width

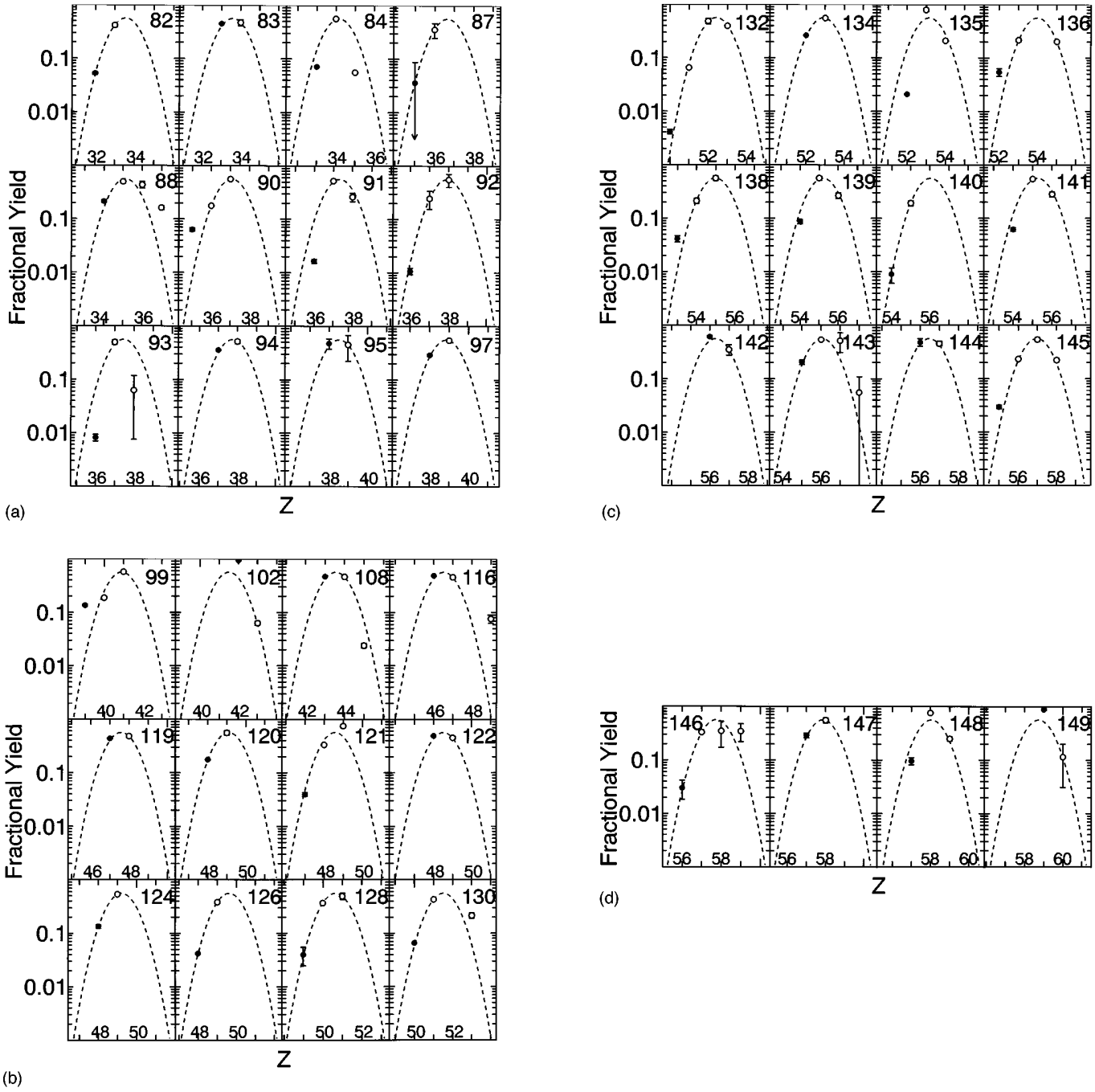

FIG. 2. Fractional yields of fission products in the 24 MeV proton-induced fission of ^{238}U. The closed symbols represent the fractional cumulative yields and the open circles indicate the independent yields. The curves are the estimated Gaussian distribution. (See text.)

parameter was treated as a free parameter. The value of the resulting width parameter which gives the best fit was $C = 1.00 \pm 0.12$ which is about the same as the reported value [2]. The Gaussian charge distribution curves calculated with the obtained Z_p and C are shown in Fig. 2 together with the relative yields of the fission products.

But in the case of light and medium mass products, there are few normalizing points. If the transport efficiency in IGISOL is regarded to be constant in a given mass chain, Z_p can be obtained directly. The Z_p obtained under such an assumption was compared with those above evaluated for heavy mass chains. The comparison shows that directly obtained Z_p's are in fair agreement with those evaluated from the calculation. As seen for $A = 128$ to 149 of Fig. 2, the calculated Gaussian curves reproduce the observed yields fairly well. Therefore, the transport efficiency may not be an important parameter in determining the gross structure of the charge distribution. Using this assumption, the most probable charges of light and medium mass chains were estimated directly from the observed yields. The evaluated most probable charges are summarized in Table II.

C. Charge polarization

It is worthwhile to examine the present results in connection with the charge polarization in fission. If the nuclear

TABLE II. The most probable charge of fission products in the system of 24 MeV proton induced fission of ^{238}U.

A	Z_p	A	Z_p
82	33.55±0.09	124	49.21±0.04
83	33.58±0.06	126	49.62±0.05
84	34.16±0.01	128	50.65±0.26
87	36.65±1.15	130	51.51±0.10
88	35.46±0.12	132	52.42±0.15
90	37.07±0.65	134	52.90±0.01
91	37.33±0.13	135	53.16±0.05
92	37.91±0.48	136	53.99±0.18
93	37.46±0.97	138	54.99±0.16
94	37.74±0.31	139	55.20±0.14
95	38.53±0.23	140	56.04±0.39
97	38.85±0.03	141	55.25±0.09
99	40.91±0.08	142	56.31±0.15
102	41.50±0.14	143	56.06±0.22
108	43.55±0.05	144	56.47±0.09
116	46.52±0.02	145	56.97±0.09
119	47.60±0.02	146	57.75±0.49
120	47.81±0.04	147	57.86±0.08
121	48.58±0.06	148	58.04±0.10
122	48.51±0.03	149	58.73±0.42

charge is uniformly distributed throughout the fission process (the UCD model), Z_p is equal to Z_{UCD}. The value of Z_{UCD} is given by

$$Z_{\mathrm{UCD}}=\left(\frac{Z_f}{A_f}\right)A',$$

where Z_f and A_f are the charge and the mass of the fissioning nucleus, respectively, and A' is the mass of the primary fission product of interest. The deviation of Z_p from Z_{UCD} is plotted in Fig. 3. The primary fragment masses A' were estimated by adding the average number of emitted neutrons [70] to the observed masses assuming that the fissioning nucleus is ^{237}Np. If no redistribution of the nuclear charge occurred during fission, Z_p would be equal to Z_{UCD}. However, Z_p mainly lies on the proton-rich side in the light fragment mass region and on the proton-deficient side in the heavy one. This observation implies that charge polarization occurs in the fission process. The nuclides of higher charge density are formed in the light fragment region and those of lower charge density are formed in the heavy fragment region. In general, the proton-to-neutron ratio of the stable nuclei decreases with increasing mass number because of the Coulomb repulsion of protons in a nucleus. Therefore, it is expected that the nuclear stability of fission fragments reflects the charge polarization in fission. From the charge conservation of the fissioning system the magnitudes of the deviation of complementary fragments should be the same but with an opposite sign, if the nuclear charges of fragments are determined before separation. This can be ascertained by superimposing the complementary light fragments to the heavy ones. The result is shown in Fig. 4, where the mass number of the heavy fragment A'_h is taken as an abscissa. In this figure, one can see that the deviations of complementary

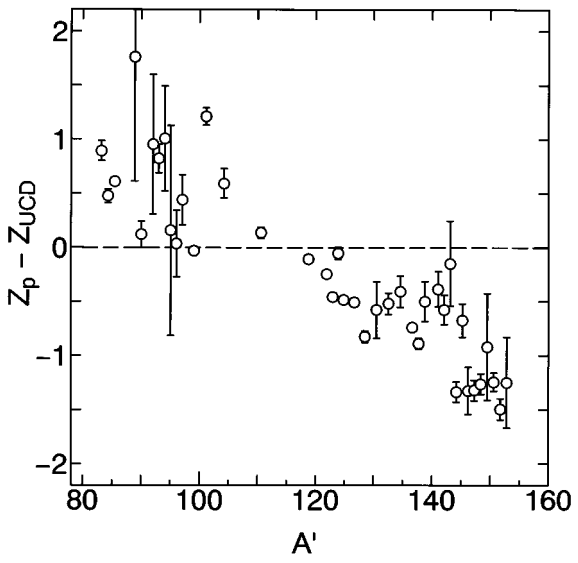

FIG. 3. Deviation of the most probable charge from that expected in the UCD model.

fragments are nearly the same. Therefore, it is suggested that the most probable charge is determined before separation. The deviation is almost negligible at symmetric mass divisions as expected. The absolute deviation tends to increase with the degree of asymmetry. But the tendency is not monotonous. Z_p abruptly approaches Z_{UCD} near the mass number $A'=142$ (or 95), beyond this region the deviation becomes large, and Z_p seems to approach Z_{UCD} again for $A'>150$ (or $A'<87$). A preference for 50-proton, 50- and 82-neutron shell effect is not clearly seen and an odd-even effect does not appear in contrast to thermal-neutron-induced and spontaneous fission [1,3,5].

The indications that the most probable charge is determined before separation and is affected by the nuclear stability suggest a certain correlation between Z_p and production Q values. For a given mass split, many combinations of charge division are possible, and the most favorable charge division may correlate with the most energetically favorable combination. This kind of interpretation is similar to the pos-

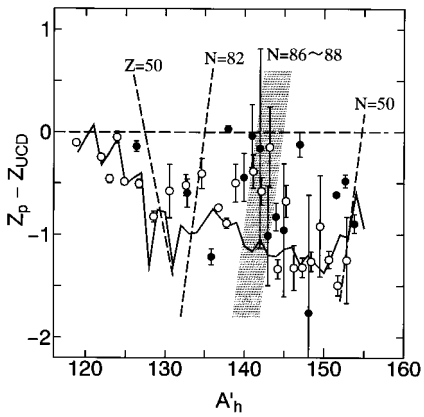

FIG. 4. Same as Fig. 3 but folded at the symmetric mass and superimposed. The light mass products are indicated by closed symbols. The solid curve is the result of the estimation using production Q values.

tulate of the minimum potential energy, MPE [11]. However, the MPE prescription is extremely sensitive to both the mass equation used and the number of emitted neutrons and, therefore, we prefer the use of ground-state masses. The most energetically favorable charge Z_{Qgg} at each mass chain was defined as the midpoint of the interpolated charges which correspond to the Q values of 5 MeV below the largest Q value, since the shape of the Q values is not a simple one. In this estimation, the Q value is defined as the difference between the mass of the fissioning nucleus and the ground-state masses of the primary fragments [71,72]. The result is shown in Fig. 4 by a solid curve. As seen in the figure, the experimental Z_p seems to correlate with the evaluated Z_{Qgg} except in the $A'=142$ region.

If the shape of the β stability curve vs the charge at a given mass number is about the same for a fragment pair, the maximum energy is available for the pair by which the differences between the most stable charge and the fragment charge are the same. In this sense, the ECD model has the similar meaning as the present consideration by the Q values. Accordingly, by a proper estimation of emitted neutrons, the ECD model may be applicable to particle-induced fission.

A sudden approach to Z_{UCD} occurs in the mass region near $A'=142$. Because this mass region is about in the middle of the neutron shell closures, any specific combinations of nuclear charges may not be pronounced, and accordingly the charge polarization is not encountered. If this is the reason for the sudden approach and the experimental Z_p is reproduced by Z_{Qgg} as seen in other mass regions, the shapes of Q_{gg} vs Z curves of this region is expected to have some indications such as a larger width or a more flattened peak. However, no such indication is observed in the shapes of the Q_{gg} vs Z curves. This mass region is coincident with the neutron closed shell of deformed nuclei, $N=86-88$, suggested by Wilkins, Steinberg, and Chasman [73]. Therefore, the deformed shell may affect the decision of the charge division, which means that the main fission path to an asymmetric mass division goes through the deformed shell.

IV. CONCLUSION

The most probable charges of 40 mass chains were determined for 24 MeV proton-induced fission of ^{238}U using IGISOL and by assuming a Gaussian charge distribution. It was found that Z_p mainly lies on the proton-rich side in the light fragment mass region and on the proton-deficient side in the heavy one; that is, the nuclides of a higher charge density are formed in the light fragment region and those of a lower charge density are formed in the heavy fragment region. This implies that charge polarization occurs in the fission process. The deviation of the most probable charge from the postulate of the unchanged charge distribution was almost equal to that of the complementary fragment at each primary mass. This means that the most probable charge is determined before separation.

The charge polarization was examined with respect to the charge Z_{Qgg} expected from the ground-state Q values. The experimental Z_p was found to be fairly well reproduced by the estimated Z_{Qgg}, which suggests that the fission reaction occurs through a minimum potential energy path. However, some structure in the differences between the experimental Z_p and Z_{UCD} was recognized at the mass region near $A'=142$. This mass region is coincident with the neutron closed shell of the deformed nuclei, $N=86-88$, suggested by Wilkins, Steinberg, and Chasman [73]. This may imply that the charge division of fission fragments is strongly affected by the deformed shell.

ACKNOWLEDGMENTS

Grateful acknowledgments are given to Y. Horikoshi, Dr. M. Wada, and Dr. H. Sunaoshi for their technical assistance during the course of the experiment. The authors thank the crews of the cyclotron of Tohoku University for their splendid cooperation with the cyclotron.

[1] A. C. Wahl, R. L. Ferguson, D. R. Nethaway, D. E. Troutner, and K. Wolfsberg, Phys. Rev. **126**, 1112 (1962).
[2] J. A. McHugh and M. C. Michel, Phys. Rev. **172**, 1160 (1968).
[3] S. Baba, H. Umezawa, and H. Baba, Nucl. Phys. **A175**, 177 (1971).
[4] A. C. Wahl, J. Radioanal. Chem. **55**, 111 (1980).
[5] A. C. Wahl, At. Data Nucl. Data Tables **39**, 1 (1988).
[6] R. H. Goeckermann and I. Perlman, Phys. Rev. **76**, 628 (1949).
[7] G. Friedlander, L. Friedman, B. Gordon, and L. Yaffe, Phys. Rev. **129**, 1809 (1963).
[8] J. H. Davies and L. Yaffe, Can. J. Phys. **41**, 762 (1963).
[9] L. E. Glendenin, C. D. Coryell, and R. E. Edwards, *Radiochemical Studies: The Fission Products* (McGraw-Hill, New York, 1951).
[10] A. C. Pappas, Paper P/881, Proceedings of the International Conference on the Peaceful Uses of Atomic Energy, Geneva, 1955.
[11] R. D. Present, Phys. Rev. **72**, 7 (1947).
[12] H. M. Blann, Phys. Rev. **123**, 1356 (1961).
[13] G. R. Choppin and E. F. Meyer, Jr., J. Inorg. Nucl. Chem. **28**, 1509 (1966).
[14] J. L. Anderson, S. H. Freid, and G. R. Choppin, J. Inorg. Nucl. Chem. **30**, 3167 (1968).
[15] G. R. Choppin and A. T. Kandil, J. Inorg. Nucl. Chem. **33**, 897 (1971).
[16] G. R. Choppin and A. T. Kandil, J. Inorg. Nucl. Chem. **34**, 439 (1972).
[17] H. Umezawa, S. Baba, and H. Baba, Nucl. Phys. **A160**, 65 (1971).
[18] S. H. Freid, J. L. Anderson, and G. R. Choppin, J. Inorg. Nucl. Chem. **30**, 3155 (1968).
[19] T. McGee, C. L. Rao, and L. Yaffe, Nucl. Phys. **A173**, 595 (1971).
[20] B. L. Tracy, J. Chaumont, R. Klapisch, J. M. Nitschke, and A. M. Poskanzer, Phys. Rev. C **5**, 222 (1972).
[21] W. Reisdorf, J. P. Unik, H. C. Griffin, and L. E. Glendenin, Nucl. Phys. **A177**, 337 (1971).
[22] J. Ärje, J. Äystö, H. Hyvönen, P. Taskinen, V. Koponen, J.

Honkanen, A. Hautojärvi, and K. Vierinen, Phys. Rev. Lett. **54**, 99 (1985).
[23] M. Yoshii, H. Hama, K. Taguchi, T. Ishimatsu, T. Shinozuka, M. Fujioka, and J. Ärje, Nucl. Instrum. Methods Phys. Res. B **26**, 410 (1987).
[24] J. F. Janni, At. Data Nucl. Data Tables **27**, 147 (1982).
[25] M. Tanikawa, H. Kudo, H. Sunaoshi, M. Wada, T. Shinozuka, and M. Fujioka, Z. Phys. A **347**, 53 (1993).
[26] M. Wada, T. Saito, H. Sunaoshi, N. Kawamura, S. Hayashibe, T. Ishimatsu, T. Shinozuka, and M. Fujioka, Nucl. Instrum. Methods Phys. Res. A **294**, 251 (1990).
[27] D. J. Morrissey, D. Lee, R. J. Otto, and G. T. Seaborg, Nucl. Instrum. Methods **158**, 499 (1979).
[28] H. W. Müller, Nucl. Data Sheets **50**, 1 (1987).
[29] J. Müller, Nucl. Data Sheets **49**, 579 (1986).
[30] H. W. Müller, Nucl. Data Sheets **56**, 551 (1989).
[31] P. Luksch and J. W. Tepel, Nucl. Data Sheets **27**, 389 (1979).
[32] H. W. Müller, Nucl. Data Sheets **54**, 1 (1988).
[33] U. Reus and W. Westmier, At. Data Nucl. Data Tables **29**, 193 (1983).
[34] H. W. Müller, Nucl. Data Sheets **31**, 181 (1980).
[35] P. Luksch, Nucl. Data Sheets **30**, 573 (1980).
[36] H. Sievers, Nucl. Data Sheets **54**, 99 (1988).
[37] H. W. Müller, Nucl. Data Sheets **44**, 277 (1985).
[38] P. Luksch, Nucl. Data Sheets **38**, 1 (1983).
[39] B. Haesner and P. Luksch, Nucl. Data Sheets **46**, 607 (1985).
[40] H. W. Müller and D. Chielewska, Nucl. Data Sheets **48**, 663 (1986).
[41] R. L. Haese, F. E. Bertland, B. Harmatz, and M. J. Martin, Nucl. Data Sheets **37**, 289 (1982).
[42] A. Hashizume, Y. Tendow, and M. Ohsha, Nucl. Data Sheets **52**, 641 (1987).
[43] B. Fogelberg and P. Hoff, Nucl. Phys. **A391**, 445 (1982).
[44] B. Fogelberg and P. Hoff, Nucl. Phys. **A376**, 389 (1982).
[45] K. Kitao, M. Kanbe, Z. Matsumoto, and T. Seo, Nucl. Data Sheets **49**, 315 (1986).
[46] T. Tamura, K. Miyano, and S. Ohya, Nucl. Data Sheets **41**, 413 (1984).
[47] T. Tamura, K. Miyano, and S. Ohya, Nucl. Data Sheets **36**, 227 (1982).
[48] K. Kitao, M. Kanbe, and Z. Matumoto, Nucl. Data Sheets **38**, 191 (1983).
[49] R. L. Auble, H. R. Hiddleston, and C. P. Browne, Nucl. Data Sheets **17**, 573 (1976).
[50] Yu. V. Sergeenkov and V. M. Sigalov, Nucl. Data Sheets **34**, 475 (1981).
[51] Yu. V. Sergeenkov, Nucl. Data Sheets **52**, 205 (1987).
[52] T. W. Burrows, Nucl. Data Sheets **52**, 273 (1987).
[53] L. K. Peker, Nucl. Data Sheets **36**, 289 (1982).
[54] L. K. Peker, Nucl. Data Sheets **32**, 1 (1981).
[55] L. K. Peker, Nucl. Data Sheets **51**, 425 (1987).
[56] L. K. Peker, Nucl. Data Sheets **45**, 1 (1985).
[57] L. K. Peker, Nucl. Data Sheets **43**, 579 (1984).
[58] L. K. Peker, Nucl. Data Sheets **48**, 753 (1986).
[59] J. K. Tuli, Nucl. Data Sheets **56**, 607 (1989).
[60] L. K. Peker, Nucl. Data Sheets **49**, 1 (1986).
[61] L. K. Peker, Nucl. Data Sheets **41**, 195 (1984).
[62] B. Sohnius, M. Brugger, H. O. Denschlag, and B. Pfeiffer, Radiochim. Acta **37**, 125 (1984).
[63] L. K. Peker, Nucl. Data Sheets **42**, 111 (1984).
[64] J. A. Szücs, M. W. John, and B. Singh, Nucl. Data Sheets **46**, 1 (1985).
[65] H. Kudo, M. Maruyama, M. Tanikawa, M. Fujita, T. Shinozuka, and M. Fujioka, Nucl. Instrum. Methods Phys. Res. B **126**, 209 (1997).
[66] R. K. Gupta, W. Scheid, and W. Greiner, Phys. Rev. Lett. **35**, 353 (1975).
[67] D. R. Saroha, R. Aroumougame, and R. K. Gupta, Phys. Rev. C **27**, 2720 (1983).
[68] J. P. Bocquet and R. Brissot, Nucl. Phys. **A502**, 213c (1989).
[69] S. Pommé, E. Jacobs, K. Persyn, D. De Frenne, K. Govaert, and M.-L. Yoneama, Nucl. Phys. **A560**, 689 (1993).
[70] M. Strecker, R. Wien, P. Plischke, and W. Scobel, Phys. Rev. C **41**, 2172 (1990).
[71] A. H. Wapstra, G. Audi, and R. Hoekastra, At. Data Nucl. Data Tables **39**, 281 (1988).
[72] J. Jänecke and P. J. Masson, At. Data Nucl. Data Tables **39**, 265 (1988).
[73] B. D. Wilkins, E. P. Steinberg, and R. R. Chasman, Phys. Rev. C **14**, 1832 (1976).